Clim Dyn
DOI 10.1007/s00382-009-0574-z

Interannual variability of the Guinea Dome and its possible link with the Atlantic Meridional Mode

Takeshi Doi · Tomoki Tozuka · Toshio Yamagata

Received: 27 May 2008 / Accepted: 6 April 2009

Abstract Using a high-resolution ocean general circulation model forced by NCEP/NCAR reanalysis data, the interannual variability of the Guinea Dome is studied from a new viewpoint of its possible link with the Atlantic Meridional Mode (AMM), which is related to the meridional migration of the Intertropical Convergence Zone (ITCZ). The dome develops off Dakar seasonally from late spring to late fall owing to the wind-induced Ekman upwelling; its seasonal evolution is associated with the northward migration of the ITCZ. When the ITCZ is located anomalously northward (southward) from late spring to early summer, as a result of the wind-evaporation-sea surface temperature (SST) positive feedback with positive (negative) SST anomaly over the Northern Hemisphere, the dome becomes unusually strong (weak) in fall as a result of stronger (weaker) Ekman upwelling. This may contribute to the decay of the AMM. Thus, the coupled nature between the AMM and the Guinea Dome could be important in understanding, modeling, and predicting the tropical Atlantic variability.

Keywords Atlantic Meridional Mode · Guinea Dome · Intertropical Convergence Zone · Interannual variability

1 Introduction

The Guinea Dome (hereafter referred to as GD) is a thermal upwelling dome in the northeastern tropical Atlantic (Rossignol and Meyrueis 1964). It is sometimes called the Dakar Dome. Its core is located near 10°N, 22°W and associated with a cyclonic circulation composed of the eastward North Equatorial Countercurrent (NECC), the eastward North Equatorial Undercurrent (NEUC), and the westward North Equatorial Current (NEC) (Mazeika 1967). Yamagata and Iizuka (1995, hereafter referred to as YI95), using an ocean general circulation model (OGCM), concluded that the GD develops in boreal summer due to the regional Ekman upwelling associated with the northward migration of the Intertropical Convergence Zone (ITCZ), and matures in fall.

In contrast to the other regions along the same latitude in the Atlantic, the sea surface temperature (SST) in the GD region is closely linked with subsurface temperature (Dewitte and Schneider 2006), and thus ocean dynamics is very important in the seasonal variation of SST (Yu et al. 2006). Since seasonal predictability of rainfall during July–September over Senegal near the GD region is known to be associated with SST anomaly (SSTA), interannual variations of the GD may be important from the regional climatic viewpoint (Moron et al. 2006). Also, the GD has a strong influence on biological activities; chlorophyll-*a* concentration is high in the GD region and linked with the intensity of the doming (Signorini et al. 1999; Pradhan et al. 2006). Pelegri et al. (2006) showed that nutrient is rich in surface during boreal fall when the GD is reinforced.

Although the interannual variations of the GD seem to be very important, they have not been understood very well so far, partly due to sparseness of observational data. Among few studies, Lazaro et al. (2005), based on the altimeter data, have suggested that the interannual positive anomaly of the GD in 1998 seems to be associated with the

T. Doi · T. Tozuka · T. Yamagata (✉)
Department of Earth and Planetary Science, Graduate School of Science, The University of Tokyo, 7-3-1 Hongo, Bunkyo-ku, Tokyo 113-0033, Japan
e-mail: yamagata@eps.s.u-tokyo.ac.jp

Published online: 21 April 2009

1997–1998 El Niño. However, its detailed mechanism is still unclear.

In the present paper, using outputs from a high-resolution OGCM, we analyze the interannual variations of the GD in detail and discuss their connection with the Atlantic Meridional Mode (AMM) through the meridional migration of the ITCZ. The content is organized as follows. In Sect. 2, a brief description of the model is given. Then, in Sect. 3, the simulated seasonal variations of the GD are compared with previous works to validate the present model results. The interannual variations of the GD are discussed in Sect. 4. The final section is reserved for summaries and discussions.

2 Model description (OFES)

The high-resolution OGCM used in this study is based on the modular ocean model (MOM3; Pacanowski and Griffies 2000), and is called OFES (OGCM for the Earth Simulator; Masumoto et al. 2004). It covers a near-global basin from 75°S to 75°N with horizontal grid spacing of 0.1°. There are 54 vertical levels with varying distance from 5 m at the surface to 330 m at the maximum depth of 6,065 m. The bottom topography is adopted from 1/30° bathymetry dataset created by the Ocean Circulation and Climate Advanced Model (OCCAM) project at the Southampton Oceanography Center (obtained through GFDL/NOAA). The viscosity and diffusivity vary in space (Smith et al. 2000) and the background horizontal bi-harmonic viscosity and diffusivity are -27×10^9 and -9×10^9 m^4 s^{-1}, respectively. The KPP boundary layer mixing scheme (Large et al. 1994) is adopted for the vertical mixing.

For the climatological seasonal integration, monthly mean climatology of wind stress data from the NCEP/NCAR reanalysis data (Kalnay et al. 1996) averaged for the period from 1950 to 1999 are used. The surface heat flux is calculated using the monthly mean climatology from the NCEP/NCAR reanalysis data by adopting the bulk formula of Rosati and Miyakoda (1988). More than half of the insolation is absorbed within a top half meter, and the remaining fraction is absorbed within upper 50 m. The fresh water flux is obtained from the same reanalysis data. In addition, the surface salinity is restored to the monthly mean sea surface salinity (SSS) of the World Ocean Atlas 1998 (WOA98; Conkright et al. 1998) with the restoring time of 6 days. It includes the contribution from the river run-off. In the sponge layer within 3° from northern and southern artificial boundaries, the temperature and salinity fields are restored to the monthly mean climatological values (WOA98) at all depths. The restoring time at those boundaries is 1 day and it increases up to the infinity in the interior region. The model is integrated for 50 years from the annual mean temperature and salinity fields (WOA98) without motion. After this climatological seasonal integration, the model is driven by the daily NCEP/NCAR reanalysis data from 1950 to 2001, with the same restoring boundary condition for SSS. We have calculated monthly climatology by averaging the model monthly data for 52 years from 1950 to 2001. In Sect. 4, we focus on the interannual variability. Therefore, we define anomaly fields as deviations from the monthly mean climatology, and variability beyond a period of 8 years has been excluded by a low-pass wavelet filter (Torrence and Compo 1998). Also, 3-month running mean is applied.

For comparison, we use the subsurface temperature data from the WOA05 (http://www.nodc.noaa.gov). Also, we use the assimilation data of Masina et al. (2004) for the horizontal velocity, the ERSSTv2 data for SSTA (Smith and Reynolds 2004), and TOPEX/Poseidon data for the sea surface height anomaly (SSHA) (http://podaac.jpl.nasa.gov/cgi-bin/dcatalog/fam_summary.pl?ost+topex).

3 Annual cycle

We find a dome-like cold region in the subsurface temperature field at a depth of 54 m from both the OFES result and the WOA05 data (Fig. 1a, b). It extends westwards from the northwestern African coast throughout a year. It is particularly distinguishable from the end of boreal summer to fall. As shown by Stramma et al. (2005), the core of the GD in summer moves northwestward in fall. The core of the strongest dome in fall is located near 12°N, 26°W. The dome-like subsurface temperature pattern is more clearly seen in vertical sections of the temperature (Fig. 2). The subsurface doming of isotherms appears more clearly in the meridional section than in the zonal section. This is because the GD is located between the westward NEC around 14°N and the eastward NECC around 9°N (Fig. 3), as Siedler et al. (1992) discussed from the hydrographic analyses.

The overall agreement between the model temperature field and the WOA data is quite good except that the model dome is about 1°C colder and extends further westward than the observational data. Also, the southeastern corner of the simulated GD is colder than the observation. YI95 showed that the coastal Guinea region experiences warming twice a year in April–July and November–December due to the coastal downwelling Kelvin wave forced by the semiannual relaxation of the trade wind in the equatorial region east of 30°W. The warm events are slightly weaker in the OFES. It may be due to the bias of the NCEP wind, where the semiannual relaxation of the trade winds is weaker.

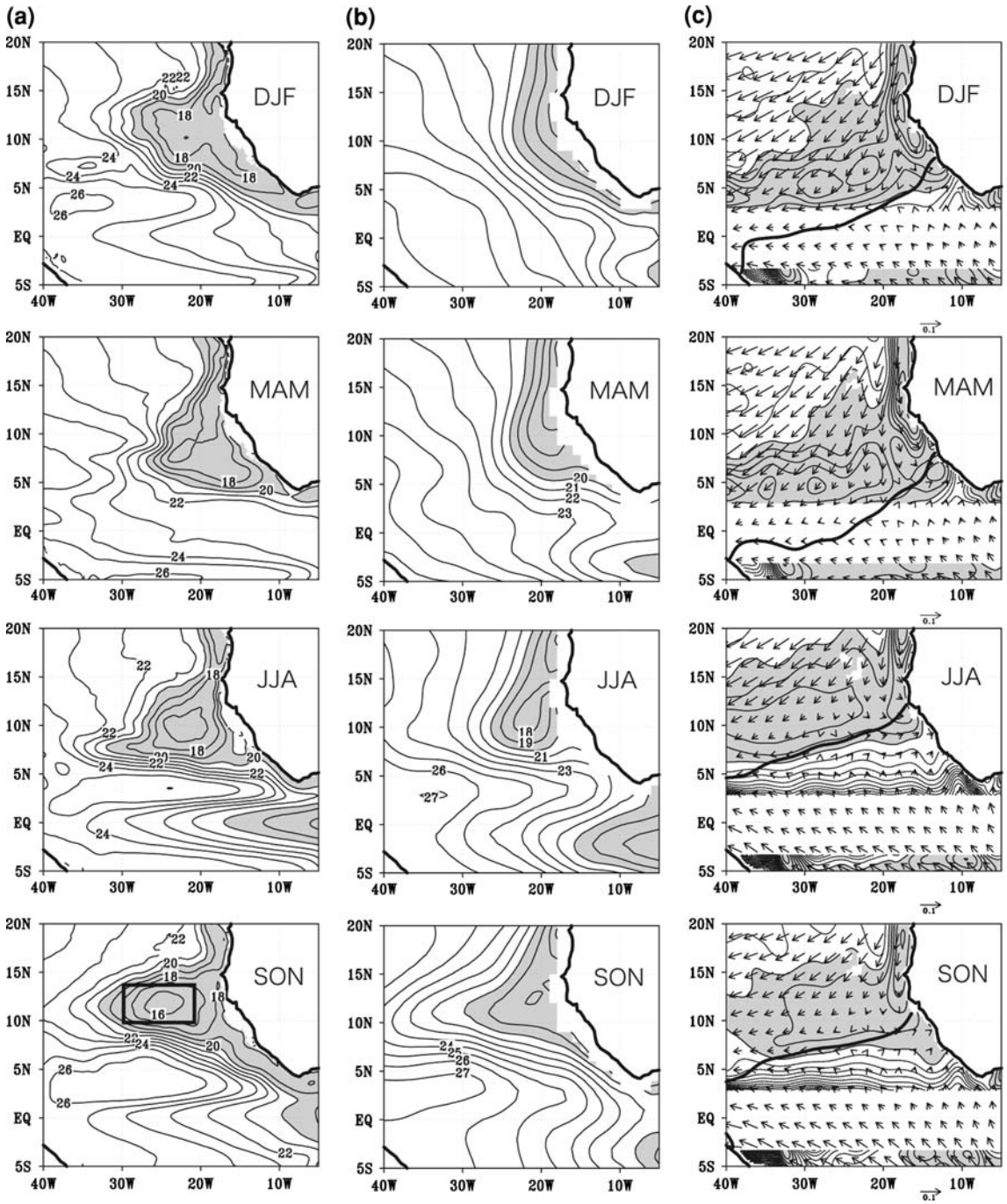

Fig. 1 Annual march of subsurface temperature at a depth of 54 m from **a** OFES and **b** WOA05. Contour interval of temperature is 1°C. Temperatures <20°C are *shaded*. The location of Region A (10°–13.5°N, 30°–21°W) is also shown in the panel for fall in **a**. **c** Wind stress and Ekman upwelling from the NCEP/NCAR reanalysis data. Magnitude of wind stress is shown by the vector drawn below figures (in N m^{-2}). Ekman upwelling is shown with contour interval of 10^{-6} m s^{-1} and areas with upwelling are *shaded* in **c**. Also, location of ITCZ, defined as zero meridional wind stress, is shown by *thick line*

Here, we consider Region A (10°–13.5°N, 21°–30°W, see Fig. 1a) that includes most of the developed dome in fall. Figure 4 shows the vertical distribution of rate of change of climatological temperature in Region A. The seasonal changes of the simulated GD are confined almost above a depth of 100 m and are most remarkable at around 50 m, as in the observation and the model results of Siedler et al. (1992) and YI95. Then, we calculate the rate of change of subsurface temperature at a depth of 54 m and vertical velocity at a depth of 58 m averaged in Region A (Fig. 5). The total rate of change is determined by three terms: the vertical heat advection, the horizontal heat

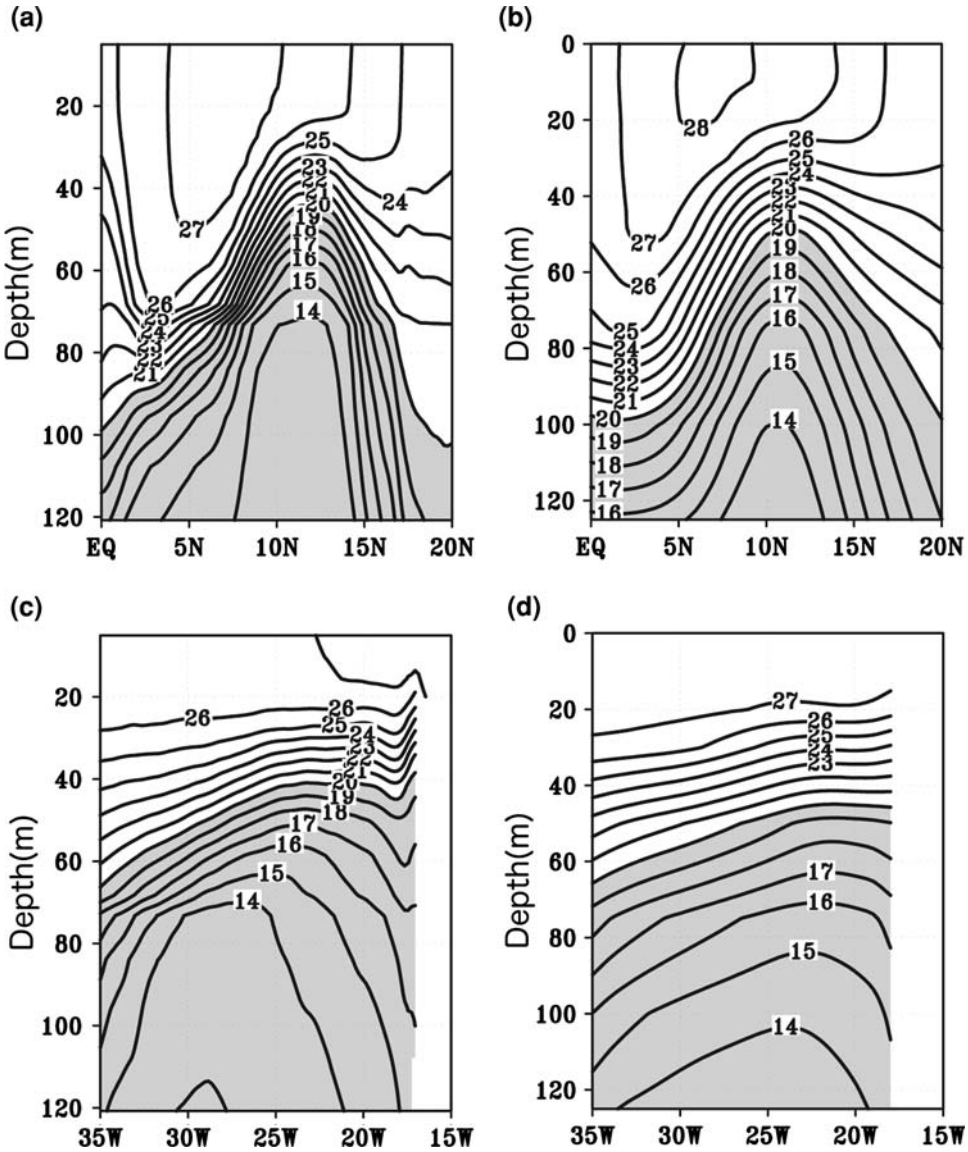

Fig. 2 **a** Temperature along meridional (26°W) section averaged from September to October from OFES. Contour interval is 1°C. Temperatures <20°C are *shaded*. **b** As in **a** but from WOA05. **c** As in **a** but along zonal (12°N) section. **d** As in **c** but from WOA05

advection, and the residual term, which is computed as the difference between the tendency term and the adiabatic heat transport terms. Thus, the latter term is mostly due to the diabatic process of mixing. Also, we assume that the model vertical velocity at the depth is composed of the regional wind-induced Ekman upwelling and the residual that is calculated by subtracting the Ekman upwelling from the model vertical velocity. Note that the latter term includes the upwelling associated with the propagation of remotely forced oceanic waves and non-linear effects.

From May through October, the subsurface temperature in Region A decreases (Fig. 5a). The vertical heat advection related to upwelling dominates the cooling with a peak in August. It is due mainly to the regional wind-induced upwelling from May to October. We note that this variation is associated with the meridional migration of the ITCZ (Fig. 1c); it is located at the southernmost latitude in April, then moves northward and reaches the northernmost location during late summer. This may explain why the center of the GD moves northwestward from summer through fall. Also, the subsurface cooling in summer is out of phase with sea surface heating (Fig. 4). Thus, the GD may provide a favorable field of absorbing heat from the atmosphere through the cold-water upwelling intensified in summer. Since the simulated seasonal variation of the GD is consistent with observation and previous image, we now focus on the interannual variation.

4 Interannual variations

Figure 6 shows the interannual variation of the subsurface temperature anomaly at a depth of 54 m, SSTA, and SSHA in Region A. The correlation between the simulated SSTA

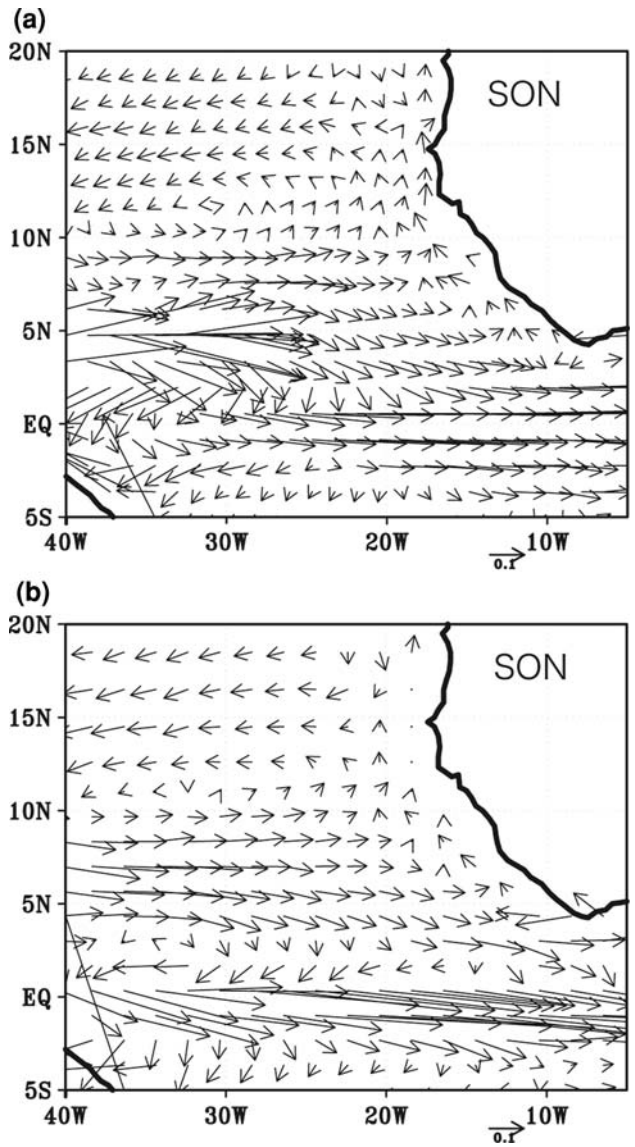

Fig. 3 **a** Subsurface horizontal velocity vectors at a depth of 54 m in the Guinea Dome region averaged from September to October from OFES. **b** As in **a** but from assimilation data of Masina et al. (2004). Unit is in m s^{-1}

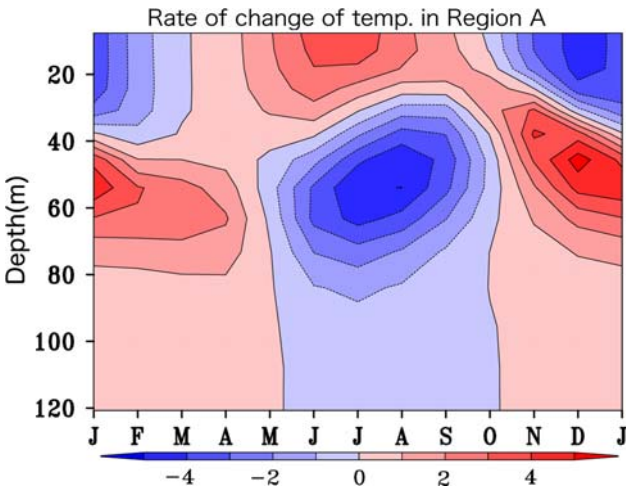

Fig. 4 Monthly rate of change of temperature in Region A (in 10^{-7} K s^{-1})

and observational SSTA in Region A is 0.84. This high correlation is expected because the model is forced by the bulk formula, which is close to a restoring formulation for latent heat flux and sensible heat flux. The correlation between the simulated SSHA and observational SSHA in Region A is 0.58. As is clear from these good correlations, we may say that the interannual variations associated with the GD are relatively well reproduced in the model. However, we note that the simulated variability of SSHA is weaker than that of observation. This model bias may be due to the forcing of NCEP/NCAR wind stress. The variability of wind stress curl of NCEP/NCAR reanalysis data is weaker than that of QuickSCAT data in Region A. Also, shown in Fig. 6a is the subsurface temperature anomaly averaged from September to November (SON), when the GD is mature on the climatological basis. To clarify the mechanism of the interannual variations, we adopt a composite analysis hereafter. As shown in Table 1, eight typical cold GD events in 1966, 1970, 1979, 1981, 1982, 1983, 1987, and 1991 and eight typical warm GD events in 1953, 1957, 1959, 1965, 1968, 1971, 1980, and 1985 are selected because the anomalies in those exceed one standard deviation (about 0.8°C) during fall (SON).

4.1 Composites for cold GD years

The GD is anomalously cooled from late boreal spring through summer, and reaches the height in fall (Fig. 7a). To understand the mechanism in detail, we have calculated the rate of change of the anomalous subsurface temperature at a depth of 54 m and the vertical velocity anomaly at a depth of 58 m in Region A in a manner similar to Fig. 5. The rate of change of the anomalous subsurface temperature is negative from March through August with the largest magnitude in May (Fig. 8a), which is due mainly to the negative vertical heat advection. It is related to anomalously strong in situ Ekman upwelling induced by the wind stress curl anomaly (Fig. 8b). This is in contrast with the situation in the Angola Dome in the South Atlantic. The interannual variation of the Angola Dome is mainly due to the downwelling Rossby waves originating from the Kelvin waves forced by the unusual relaxation of trade winds in the central equatorial Atlantic (Doi et al. 2007).

As shown in Fig. 9a, the stronger Ekman upwelling in Region A is related to the anomalously northward migration of the ITCZ from spring to early summer. This is associated with the warm SSTA in the northern off-equatorial region during this season (Fig. 7b). Thus, the warm

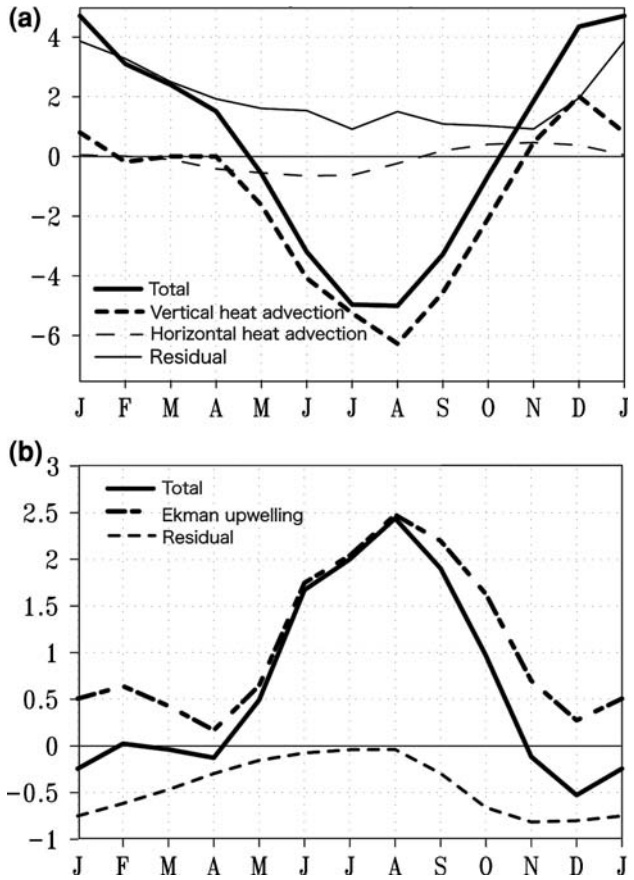

Fig. 5 **a** Rate of change of temperature at a depth of 54 m: total rate of change ("Total") is determined by vertical heat advection, horizontal heat advection, and residual term for Region A (in 10^{-7} K s^{-1}). **b** Modeled vertical velocity at a depth of 58 m: modeled vertical velocity ("Total") is determined by regional-wind induced Ekman upwelling and residual for Region A (in 10^{-6} m s^{-1})

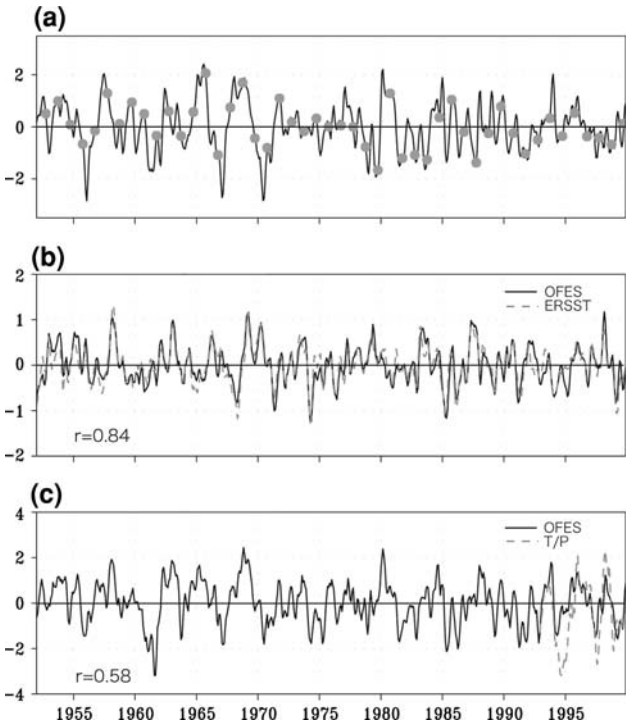

Fig. 6 **a** Subsurface temperature anomaly (in °C) at a depth of 54 m in Region A. The anomalies averaged from September to November are shown by *filled cycles*. **b** SSTA (in °C) for OFES (*solid line*) and ERSSTv2 (*thin dashed line*) in Region A. **c** SSHA (in 10^{-2} m) for OFES (*thick line*) and TOPEX/Poseidon (*thin dashed line*) in Region A. Correlation between OFES data and observational data is shown in **b** and **c**

Table 1 Years of anomalously cold and warm events of the Guinea Dome considered in the composite analyses

Years of cold Guinea Dome	Years of warm Guinea Dome
1966	1953
1970	1957
1979	1959
1981	1965
1982	1968
1983	1971
1987	1980
1991	1985

SSTA in spring leads to the cold subsurface temperature anomaly in summer and fall. The unusual warming of SST from late winter to spring is explained mainly by the positive latent heat flux anomaly associated with the weaker evaporation owing to the weakened wind in spring (Fig. 9); the anomalously northward migration of the ITCZ is responsible for the southwesterly wind anomaly over Region A and the weakening of the trade winds there. This warming enhances the meridional gradient of SSTA and results in further anomalously northward migration of the ITCZ. This process is a typical example of the wind-evaporation-SST (WES) feedback as discussed by Xie (1999). Since our model is forced by the bulk formula, further studies using a coupled general circulation model are necessary to discuss the coupled feedback in details. Breugem et al. (2007) showed that the northern tropical Atlantic variability is closely linked with the WES feedback by use of an atmospheric general circulation model coupled to a passive mixed layer model for the ocean. It is consistent with results from coupled general circulation models by Huang and Shukla (2005) and Breugem et al. (2006).

The WES feedback develops not only owing to the warm SSTA in the Northern Hemisphere, but also owing to the cold SSTA in the Southern Hemisphere just as a mirror image of the above; the northward migration of the ITCZ causes the southeasterly wind anomaly in the Southern Hemisphere in spring, leading to the stronger trade winds and promotion of the evaporation (Figs. 7, 9). This meridional SSTA dipole is known as the AMM, which was

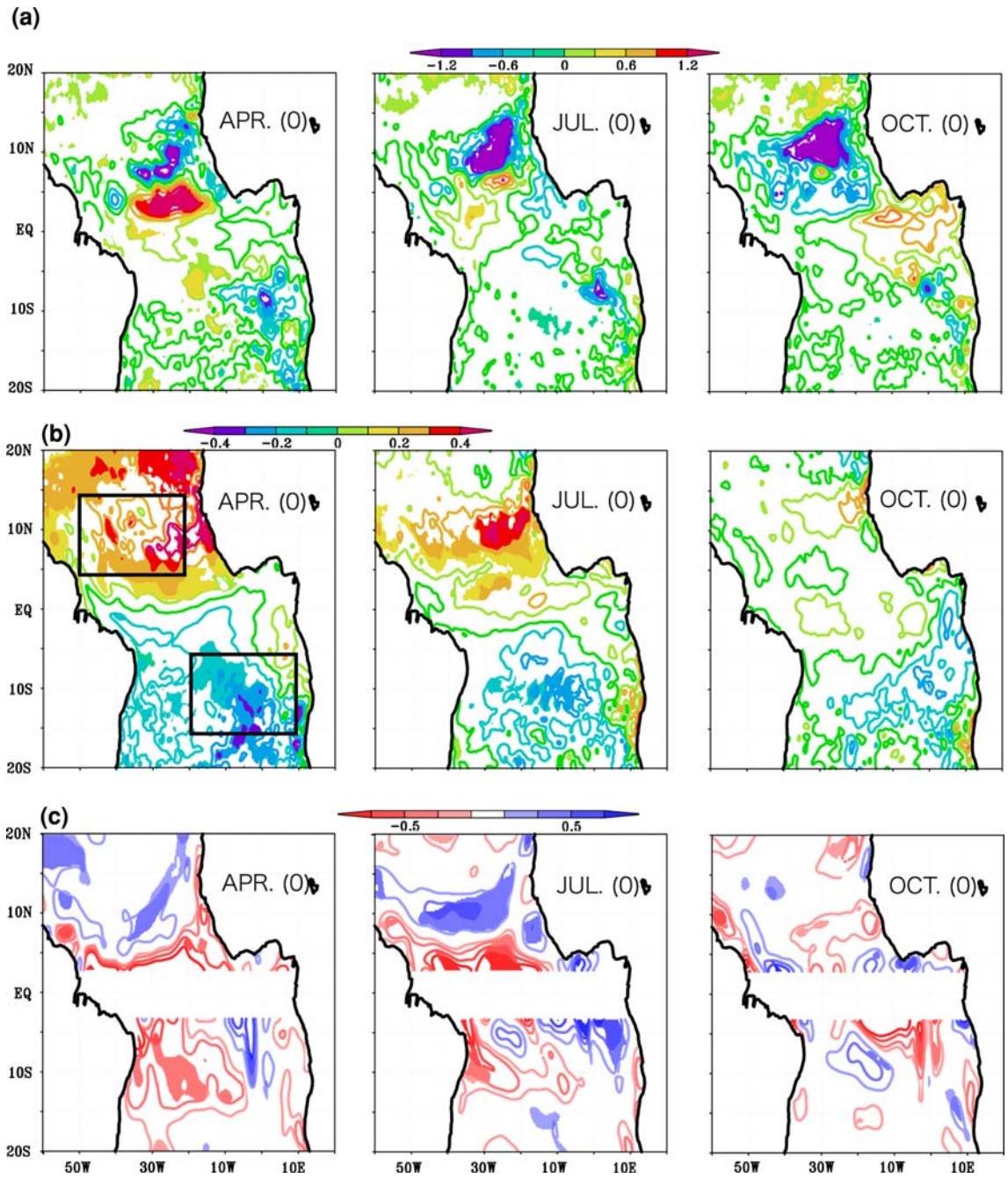

Fig. 7 Anomalous **a** subsurface temperature at a depth of 54 m (in °C), **b** SST (in °C), and **c** Ekman upwelling (in 10^{-6} m s^{-1}) for eight cold GD years (1966, 1970, 1979, 1981, 1982, 1983, 1987, and 1991). 0 indicates the cold GD years. Contour interval is 0.3°C for subsurface temperature, 0.1°C for SST, and 0.25 × 10^{-6} m s^{-1} for Ekman upwelling. Anomalies above 90% significance level are *shaded*

originally identified by Servain (1991) using a principal component analysis. The AMM develops in spring through the WES feedback, and has a great impact on Atlantic climate conditions interannually and decadally (Chang et al. 1997). Although some papers inferred that the AMM was a statistical artifact due to the assumption of spatial orthogonality in the principal component (Enfield et al. 1999; Dommenget and Latif 2000), Kushnir et al. (2006) confirmed the presence of the AMM from the regression analysis of the precipitation data (see Xie and Carton 2004 for the recent review of the AMM). Since the dipole pattern of SSTA is obtained from the composite analysis based on the interannual variation of the GD in fall, our result further supports the existence of the AMM.

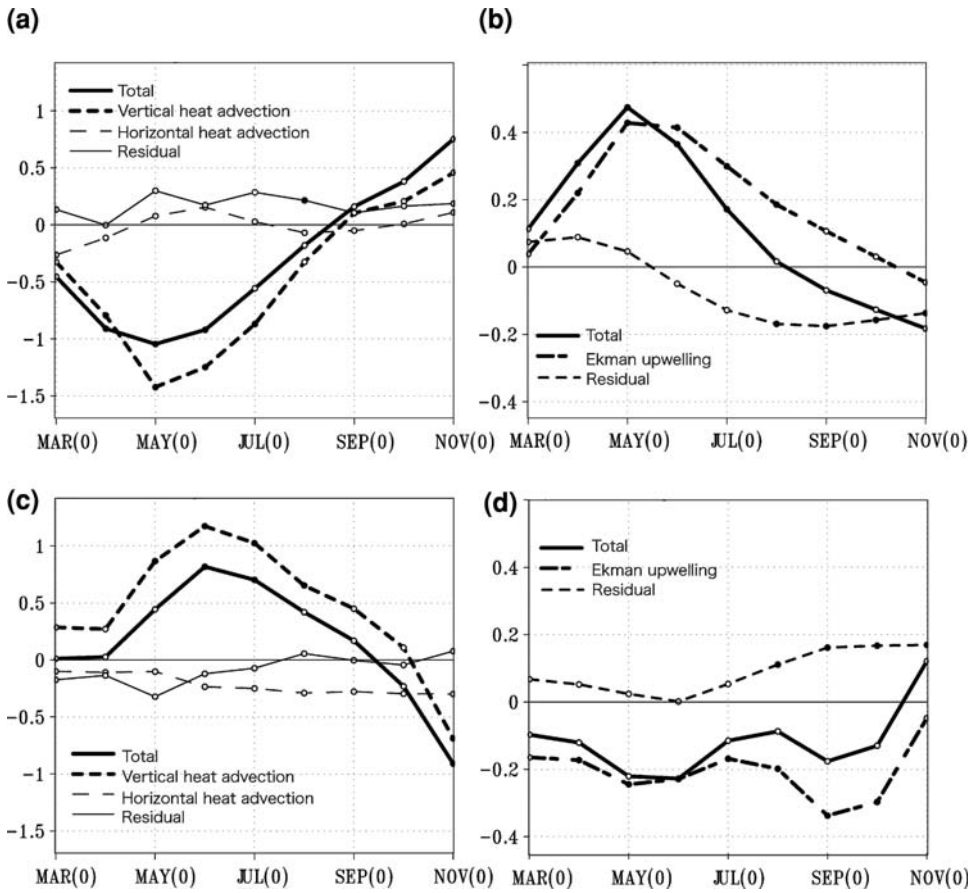

Fig. 8 **a** As in Fig. 5a, but for anomalous rate of change for eight cold GD years (in 10^{-7} K s^{-1}). **b** As in Fig. 5b, but for vertical velocity anomaly for eight cold GD years (in 10^{-6} m s^{-1}). **c** As in **a** but for eight warm GD years. **d** As in **b** but for eight warm GD years. Anomalies above 90% significance level are shown by *filled circles*

Both the meridional gradient of SSTA and the anomalously northward migration of the ITCZ are seen clearly in six (1966, 1970, 1979, 1981, 1983, and 1987) out of eight typical cold GD years (1966, 1970, 1979, 1981, 1982, 1983, 1987, and 1991), although the positive SSTA in the Northern Hemisphere is much stronger than the negative SSTA in the Southern Hemisphere in 1966 and 1979. In 2 years (1982 and 1983), the anomalously northward migration of the ITCZ seems to be also related with the Atlantic Niña (Zebiak 1993). This possible relationship between the AMM and the Atlantic Niño/Niña is interesting (Servain et al. 1999). However, the statistical significance is too low to discuss it in detail. The cold GD in 1991 is an exceptional case because the GD is cold already in winter of the previous year.

4.2 Composites for warm GD years

The GD is warmed anomalously from April through September and reaches its height in fall (Figs. 8c, 10a). The vertical heat advection associated with the Ekman downwelling anomaly excited by the weakened positive curl of the wind stress seems to be responsible for this warming at least up to early summer (Figs. 8d, 10c). This is because the vertical velocity anomaly is well explained by the in situ Ekman downwelling anomaly during the period. The wind anomaly is due to the anomalously southward migration of the ITCZ during spring (Fig. 11a). As seen in the SSTA field in Fig. 10b, the negative SSTA in the Northern Hemisphere during this season is responsible for the ITCZ migration. The unusual cooling in the Northern Hemisphere is explained mainly by the enhanced latent heat loss from January through May, which is associated with the stronger evaporation caused by the stronger wind (Fig. 11). This cooling enhances the meridional gradient of SSTA and results in further anomalously southward migration of the ITCZ.

Thus, the composite for the warm GD years is almost a mirror image of that of the cold GD years, and the meridional gradient of SSTA in spring is responsible for the anomalously warm GD in fall through the anomalously southward migration of the ITCZ. This is clearly seen in seven (1953, 1957, 1959, 1965, 1968, 1971, and 1985) out of eight warm GD years (1953, 1957, 1959, 1965, 1968, 1971, 1980, and 1985), although the anomalously southward migration of the ITCZ seems to be also related to

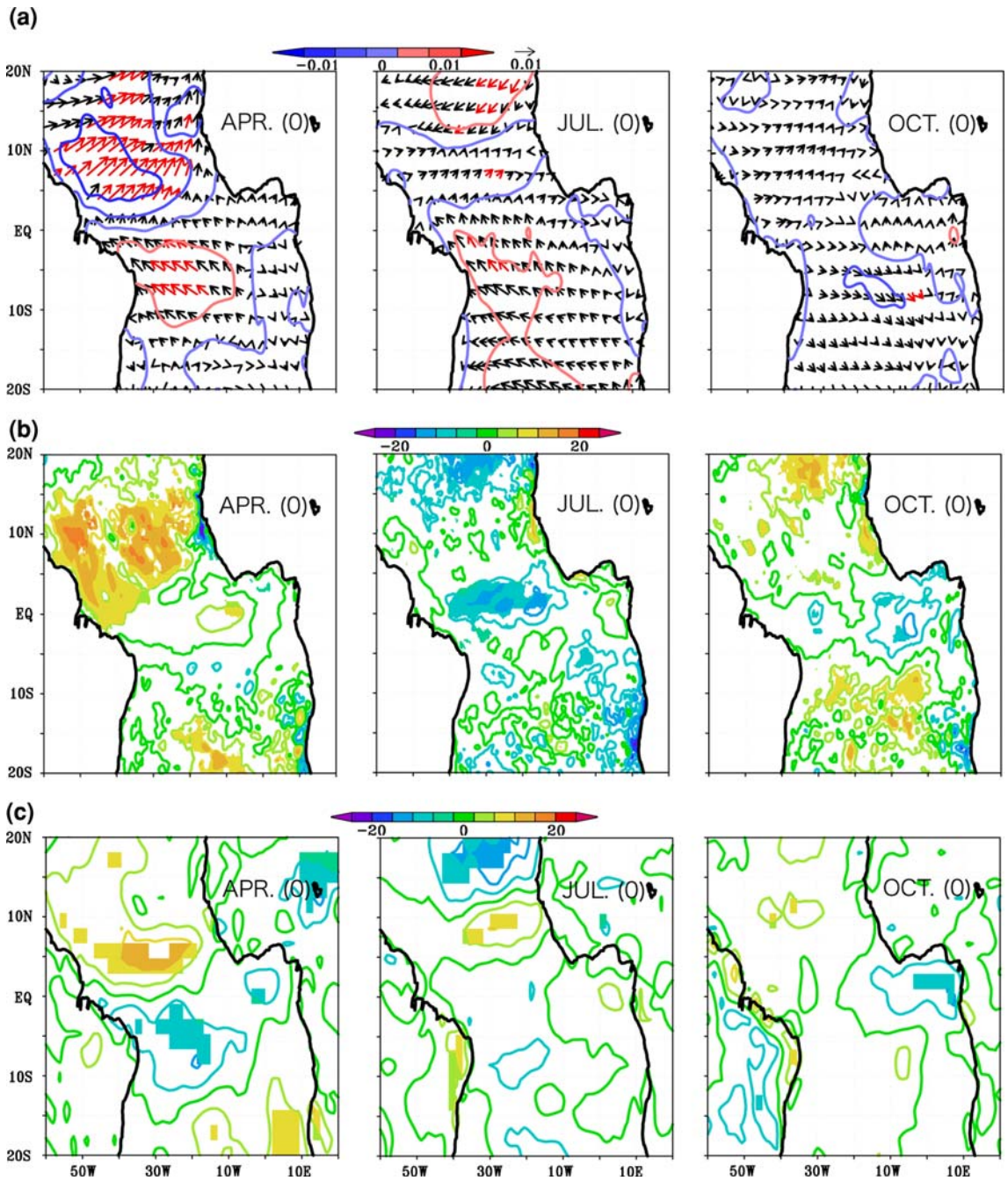

Fig. 9 As in Fig. 7 but for anomalous **a** wind stress (in N m^{-2}), **b** sea surface heat flux (in W m^{-2}), and **c** latent heat flux (in W m^{-2}). Contour interval for wind stress is 0.005 N m^{-2}, and that for the surface and latent heat flux is 5 W m^{-2}

Atlantic Niño during summer in 1957 and 1968. In 1980, the GD is anomalously warm already from the previous winter.

4.3 Possible impact of the GD on the AMM

Figure 12 shows the interannual variation of the AMM index (AMMI), which is defined as the difference between the northern index (SSTA in 5–15°N, 50°–20°W) and the southern index (SSTA in 5–15°S, 20°W–10°E) (for locations; see Fig. 7b). We note that the correlation between the AMMI derived from the OFES and that from the ERSSTv2 is 0.85, which means the present model captures the AMM in the real ocean rather well. The correlation between the AMMI from the OFES averaged from March to May and the subsurface temperature anomaly in Region A averaged from SON is −0.46, which is significant above 99% confidence level based on the *t* test. Thus, we may

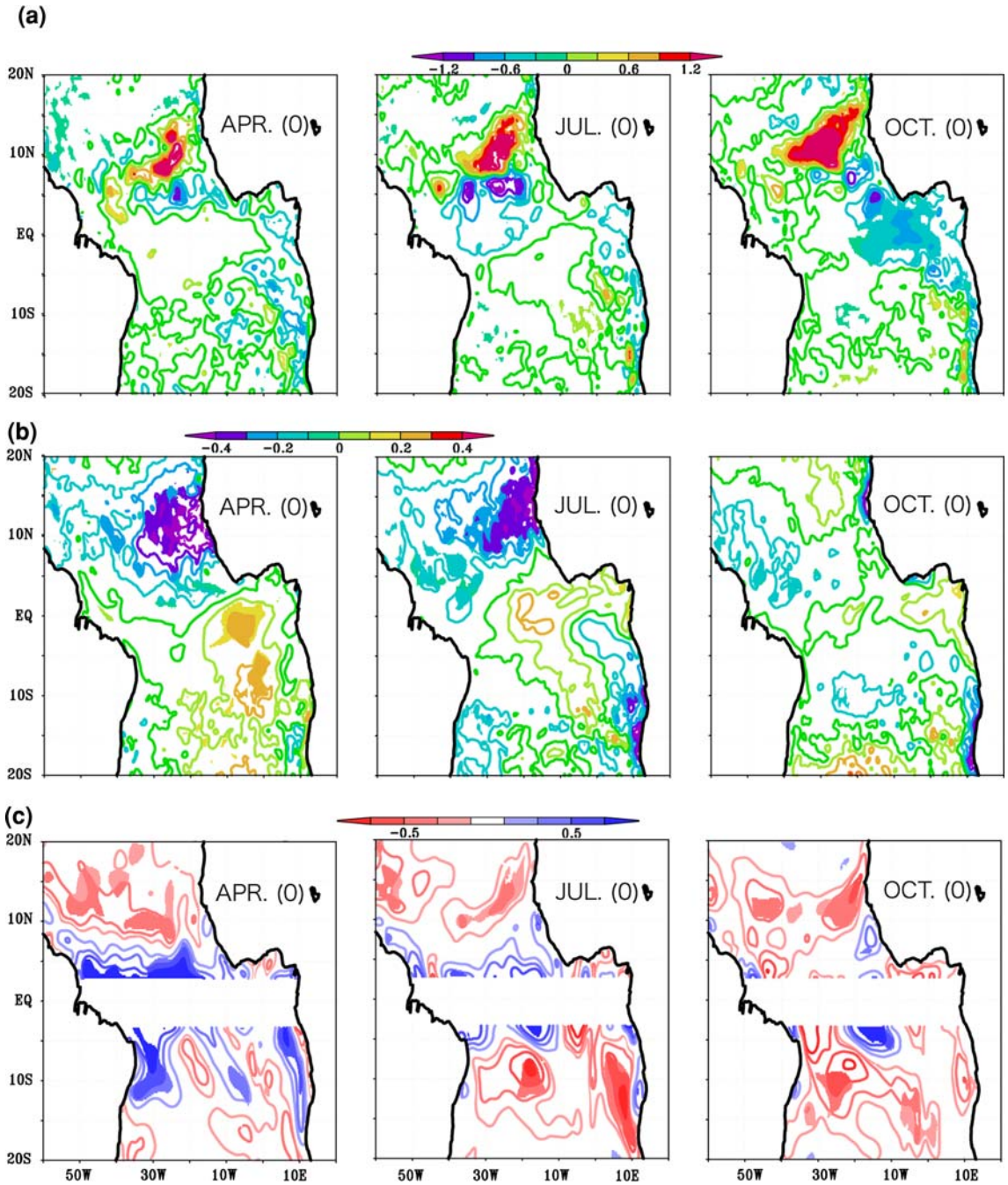

Fig. 10 As in Fig. 7 but for eight warm GD years (1953, 1957, 1959, 1965, 1968, 1971, 1980, and 1985)

conclude that both positive and negative phases of the AMM that develops in spring are related to the interannual variations of the oceanic GD in fall through the meridional migration of the ITCZ. This link is also identified from the composite method based on the typical AMM years. This involvement of the ocean dynamics in the AMM needs to be paid more attention.

In order to further demonstrate a possible connection between the subsurface temperature and SST, we have calculated the heat budget anomaly for the upper 58 m over Region A (Fig. 13). The temperature averaged above a depth of 58 m increases anomalously from March to April in the cold GD years. This warming is mainly due to positive sea surface heat flux anomaly. In contrast, the anomalous cooling from May to September is due to vertical heat advection. For the warm GD years, the anomalous cooling from March to April is due to negative surface heat flux anomaly, and the mean temperature of the

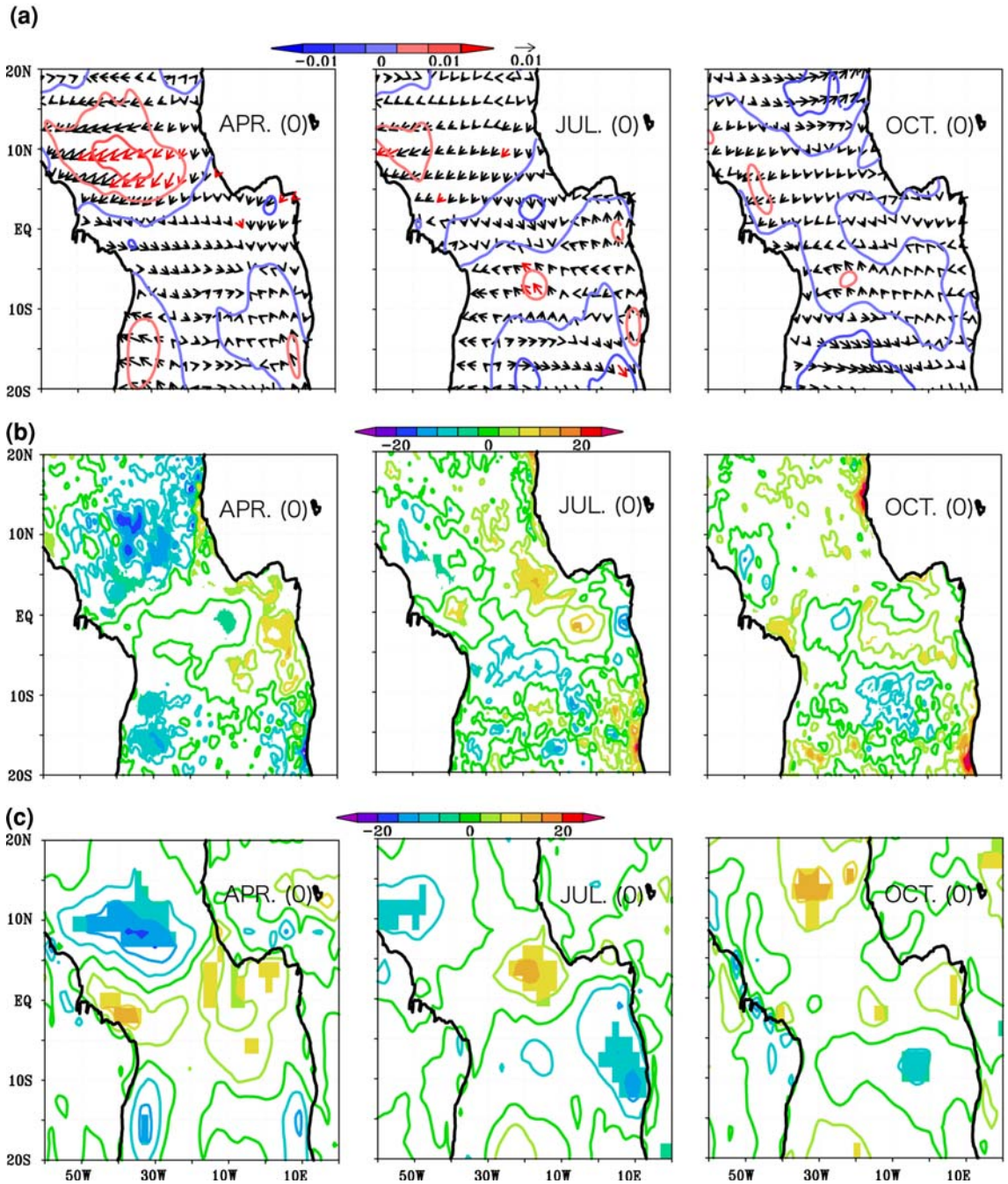

Fig. 11 As in Fig. 9 but for eight warm GD years

upper 58 m is anomalously warmed from May to October by the vertical heat advection. We note that the horizontal heat transport is not important to the heat budget. Thus, the retreat of the positive (negative) temperature anomaly above a depth of 58 m over Region A during summer is due to intensified (weakened) upwelling associated with the anomalously cool (warm) GD. Therefore, the ocean–atmosphere interaction including the variation in the subsurface temperature of the GD could be important in the decay of the AMM, even though past studies on the AMM discussed only the atmospheric forcing.

5 Summary and discussion

Using outputs from the high-resolution OGCM, the interannual variation of the oceanic conditions of the GD is investigated in detail. The GD develops off Dakar

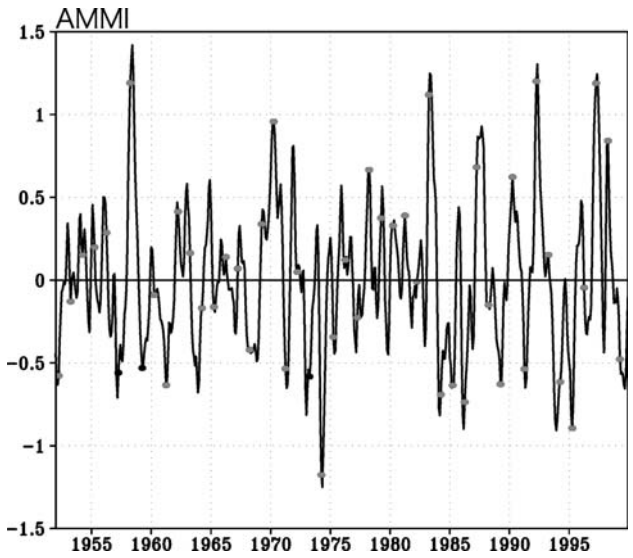

Fig. 12 Atlantic meridional mode index (AMMI) from OFES (in °C), which is defined as the SSTA averaged in the northern region (5–15°N, 50°–20°W) minus that in the southern region (5–15°S, 20°W–10°E) (*thick line*). The values averaged from March to May (MAM) are also show by *filled cycles*

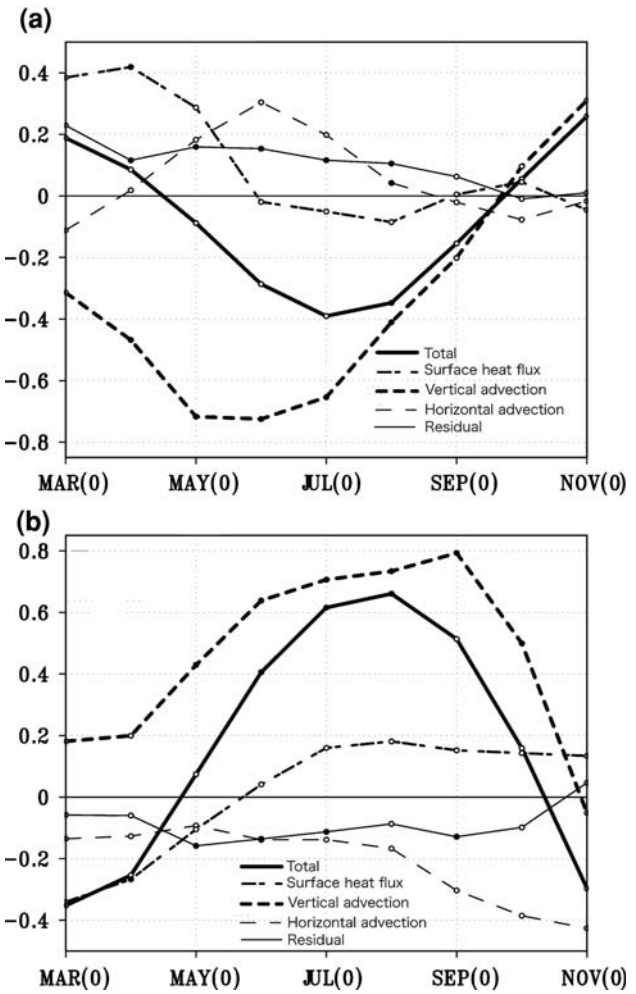

Fig. 13 **a** Heat budget anomaly in the upper 58 m over Region A for the cold GD years (in 10^{-7} K s^{-1}). Total rate of change ("Total") is determined by sea surface heat flux, vertical heat advection, horizontal heat advection, and residual term. **b** As in **a** but for eight warm GD years. Anomalies above 90% significance level are shown by *filled circles*

seasonally from late spring to late fall owing to the wind-induced Ekman upwelling associated with the northward migration of the ITCZ, but it shows large interannual variability. We find that interannual subsurface temperature variations of the GD in boreal fall are significantly correlated with the AMM in spring. When the ITCZ is located anomalously north (south) from late spring to early summer, the GD becomes unusually cold (warm) as a result of the upwelling (downwelling) anomaly associated with the positive (negative) wind stress curl anomaly. The northward (southward) migration of the ITCZ is due to the WES feedback mechanism in spring above the positive (negative) SST anomalies in the northern tropics. Thus, the cold (warm) subsurface temperature anomaly in summer and fall is associated with the SSTA of an opposite sign. This interesting connection is found in this study for the first time. Also, the retreat of the positive (negative) heat content above a depth of 58 m in summer is not due to the sea surface heat flux, but due to the vertical heat transport associated with the anomalously cold (warm) GD. Thus, the decay of the AMM seems to be related to the GD. However, the coupled nature still remains a hypothesis at this stage because the present model has the weaknesses that the humidity, air–temperature and wind cannot interact with ocean variables. Further studies using an ocean–atmosphere coupled general circulation model (CGCM) are necessary to investigate the air–sea interaction processes involving the GD in more detail; the work in this direction is underway.

To reveal the origin of the initial SSTA also needs further investigation. We have noticed that the southeasterly (northwesterly) wind anomaly in the Southern Hemisphere appears initially in January of the cold (warm) GD years (figure not shown). It may lead to anomalously northward (southward) migration of the ITCZ, and thus the southwesterly (northeasterly) wind anomaly in the Northern Hemisphere in spring. It may be associated with the intensification of the subtropical high in the Southern Hemisphere. Barreiro et al. (2004) suggested that the cross-equatorial gradient is pre-conditioned by the southern tropics. Also, the effects of the ENSO and the North Atlantic Oscillation (NAO) on the trigger of the AMM were discussed by Chiang and Vimont (2004) and Barreiro et al. (2005). In addition, the AMM may be preconditioned by regional mixed-layer depth anomaly in the GD region. Further studies are necessary to clarify the onset of the AMM. The work in this direction is also underway by using a CGCM.

All interannual variations of the GD cannot be explained by the above mechanism. In years such as 1956 and 1970 (1977), when the GD is anomalously cold (warm) from December of the previous year to February of this year, it seems that the positive SSTA appears only in the Northern Hemisphere during this season, instead of the meridional SSTA dipole. The monopole behavior of the SSTA may be related with the NAO (Ruiz-Barradas et al. 2000). Also, in years such as 1994 (1966), the GD is anomalously warm (cold) from December of the previous year. The Atlantic Niño2 (Niña2), which is similar to the Atlantic Niño (Niña) but peaks in boreal winter (Okumura and Xie 2006), may be involved in those events.

We note that the Atlantic Niño is the main cause of the interannual variation in the Angola Dome (Doi et al. 2007), but not for that of the GD. The correlation between the subsurface temperature anomaly at a depth of 54 m during fall in the GD and SSTA during summer in ATL3 (20°W–0°E, 3°S–3°N) is not significant. Also, the link is not identified from the composite analysis based on the typical Atlantic Niño/Niña years. The meridional asymmetry of the coastline in the eastern Atlantic basin may introduce differences in the propagation of coastal Kelvin waves originating from the tropics (e.g. Busalacchi and Picaut 1983; Schouten et al. 2005). However, strong events such as the 1963 and 1984 Atlantic Niño (1958 and 1997 Niña) seem to have influenced the anomalous warming (cooling) of the GD during summer not only through the anomalously southward (northward) movement of the ITCZ, but also through propagation of the coastal Kelvin waves along the West Africa.

The ocean dynamics in the GD region may play an important role on determining the SST through variations of the thermocline depth and the vertical heat transport. To clarify the role of the GD could be important not only for the AMM study itself, but also for the study of the regional climate in surrounding countries. We believe the efforts will also contribute to improvement of prediction of the Atlantic climate conditions by use of a coupled ocean–atmosphere model.

Acknowledgments We thank H. Sasaki and Y. Masumoto for the OFES data, which was run on the Earth Simulator Center of Japan Agency for Marine-Earth Science and Technology. The present research is supported by the Japan Society for Promotion of Science (JSPS) through Grant-in-Aid for Scientific Research B (20340125). Also, the first author is supported by the Research Fellowship of the JSPS for Young Scientists (208479). Wavelet software was provided by C. Torrence and G. Compo, and is available at http://atoc.colorado.edu/research/wavelets/.

References

Barreiro M, Giannini A, Chang P, Saravanan R (2004) On the role of the South Atlantic atmospheric circulation in tropical Atlantic variability. In Earth's climate: the ocean-atmosphere interaction. Geophys Monogr Ser 147:143–156

Barreiro M, Chang P, Ji L, Saravanan R, Giannini A (2005) Dynamic elements of predicting boreal spring tropical Atlantic sea-surface temperatures. Dyn Atmos Oceans 39:61–85. doi:10.1016/j.dynatmoce.2004.10.013

Breugem WP, Hazeleger W, Haarsma RJ (2006) Multi-model study of tropical Atlantic variability and change. Geophys Res Lett. doi:10.1029/2006GL027831

Breugem WP, Hazeleger W, Haarsma RJ (2007) Mechanisms of northern tropical Atlantic variability and response to CO_2 doubling. J Clim 20:2691–2705. doi:10.1175/JCLI4137.1

Busalacchi AJ, Picaut J (1983) Seasonal variability from a model of the tropical Atlantic ocean. J Phys Oceanogr 13:1564–1588. doi:10.1175/1520-0485(1983)013<1564:SVFAMO>2.0.CO;2

Chang P, Ji L, Li H (1997) A decadal climate variation in the tropical Atlantic ocean from thermodynamic air-sea interactions. Nature 385:516–518. doi:10.1038/385516a0

Chiang JCH, Vimont DJ (2004) Analogous Pacific and Atlantic meridional modes of tropical atmosphere-ocean variability. J Clim 17:4143–4158. doi:10.1175/JCLI4953.1

Conkright ME et al (1998) World ocean database 1998 documentation and quality control. Available via DIALOG. http://www.nodc.noaa.gov/OC5/WOA98F/woaf_cd/doc/readme.html of subordinate document. Accessed 23 May 2008

Dewitte DG, Schneider EK (2006) Diagnosing the annual cycle modes in the tropical Atlantic ocean using a directly coupled atmosphere-ocean GCM. J Clim 19:5319–5342. doi:10.1175/JCLI3888.1

Doi T, Tozuka T, Sasaki H, Masumoto Y, Yamagata T (2007) Seasonal and interannual variations of oceanic conditions in the Angola Dome. J Phys Oceanogr 37:2698–2713. doi:10.1175/2007JPO3552.1

Dommenget D, Latif M (2000) Interannual to decadal variability in the tropical Atlantic. J Clim 13:777–792. doi:10.1175/1520-0442(2000)013<0777:ITDVIT>2.0.CO;2

Enfield DB, Mestas-Nunez DA, Mayer MA, Serrano CL (1999) How ubiquitous is the dipole relationship in tropical Atlantic sea surface temperatures. J Geophys Res 104:7841–7848. doi:10.1029/1998JC900109

Huang B, Shukla J (2005) Ocean-atmosphere interactions in the tropical and subtropical Atlantic ocean. J Clim 18:1652–1672. doi:10.1175/JCLI3368.1

Kalnay E et al (1996) The NCEP/NCAR 40-year reanalysis project. Bull Am Meteorol Soc 77:437–471. doi:10.1175/1520-0477(1996)077<0437:TNYRP>2.0.CO;2

Kushnir Y, Robinson WA, Chang P, Robertson AW (2006) The physical basis for predicting Atlantic sector seasonal to interannual climate variability. J Clim 19:5949–5970. doi:10.1175/JCLI3943.1

Large WG, McWilliams JC, Doney SC (1994) Oceanic vertical mixing: a review and a model with a nonlocal boundary layer parameterization. Rev Geophys 32:363–403. doi:10.1029/94RG01872

Lazaro C, Fernandes MJ, Santos AMP, Oliverira P (2005) Seasonal and interannual variability of surface circulation in the Cape Verde region from 8 years of merged T/P and ERS-2 altimeter data. Remote Sens Environ 98:45–62. doi:10.1016/j.rse.2005.06.005

Masina S, Pietro PD, Navarra A (2004) Interannual-to-decadal variability of the North Atlantic from an ocean data assimilation system. Clim Dyn 23:531–546. doi:10.1007/s00382-004-0453-6

Masumoto Y, Sasaki H, Kagimoto T, Komori N, Ishida A, Sasai Y, Miyama T, Motoi T, Mitsudera H, Takahashi K, Sakuma H, Yamagata T (2004) A fifty-year eddy-resolving simulation of the

world ocean–preliminary outcomes of OFES (OGCM for the earth simulator). J Earth Simul 1:35–56

Mazeika PA (1967) Thermal domes in the eastern tropical Atlantic Ocean. Limnol Oceanogr 12:537–539

Moron V, Robertson AW, Ward MN (2006) Seasonal predictability and spatial coherence of rainfall characteristics in the tropical setting of Senegal. Mon Weather Rev 134:3248–3262. doi:10.1175/MWR3252.1

Okumura Y, Xie SP (2006) Some overlooked features of tropical Atlantic climate leading to a new Niño-like phenomenon. J Clim 19:5859–5874. doi:10.1175/JCLI3928.1

Pacanowski RC, Griffies SM (2000) MOM 3.0 manual. Available via DIALOG. http://www.gfdl.gov/~smg/MOM/web/guide_parent/guide_parent.html of subordinate document. Accessed 23 May 2008

Pelegri JL, Marrero-Diaz A, Ratsimandresy AW (2006) Nutrient irrigation of the North Atlantic. Prog Oceanogr 70:366–406. doi:10.1016/j.pocean.2006.03.018

Pradhan Y, Lavender SJ, Hardman-Mountford NJ, Aiken J (2006) Seasonal and inter-annual variability of chlorophyll-a concentration in the Mauritanian upwelling: observation of an anomalous event during 1998–1999. Deep Sea Res Part II Top Stud Oceanogr 53:1548–1559. doi:10.1016/j.dsr2.2006.05.016

Rosati A, Miyakoda K (1988) A general circulation model for upper ocean circulation. J Phys Oceanogr 18:1601–1626. doi:10.1175/1520-0485(1988)018<1601:AGCMFU>2.0.CO;2

Rossignol M, Meyrueis AM (1964) Campagnes oceanographiques du Gerad-Treca, Cent. Oceanogr. Dakar-Thiaroye, ORSTOM, Dakar, Senegal, p 53

Ruiz-Barradas A, Carton JA, Nigam S (2000) Structure of interannual-to-decadal climate variability in the tropical Atlantic sector. J Clim 13:3285–3297. doi:10.1175/1520-0442(2000)013<3285:SOITDC>2.0.CO;2

Schouten MW, Matano RP, Strub TP (2005) A description of the seasonal cycle of the equatorial Atlantic from altimeter data. Deep Sea Res Part I Oceanogr Res Pap 52:477–493. doi:10.1016/j.dsr.2004.10.007

Servain J (1991) Simple climatic indices for the tropical Atlantic-ocean and some applications. J Geophys Res 96:15137–15146. doi:10.1029/91JC01046

Servain J, Wainer I, McCreary JP, Dessier A (1999) Relationship between the equatorial and meridional modes of climate variability in the tropical Atlantic. Geophys Res Lett 26:485–488. doi:10.1029/1999GL900014

Siedler G, Zangenberg N, Onken R (1992) Seasonal changes in the tropical Atlantic circulation: observation and simulation of the Guinea Dome. J Geophys Res 97:703–715. doi:10.1029/91JC02501

Signorini SR, Murtugudde RG, McClain CR, Christian JR, Picaut J, Busalacchi AJ (1999) Biological and physical signatures in the tropical and subtropical Atlantic. J Geophys Res 104:18367–18382. doi:10.1029/1999JC900134

Smith TM, Reynolds RW (2004) Improved extended reconstruction of SST (1854–1997). J Clim 17:2466–2477. doi:10.1175/1520-0442(2004)017<2466:IEROS>2.0.CO;2

Smith RD, Maltrud ME, Bryan FO, Hecht MW (2000) Numerical simulation of the North Atlantic Ocean at 1/10. J Phys Oceanogr 30:1532–1561. doi:10.1175/1520-0485(2000)030<1532:NSOTNA>2.0.CO;2

Stramma L, Huttl S, Schafstall J (2005) Water masses and currents in the upper tropical northeast Atlantic off northwest Africa. J Geophys Res. doi:10.1029/2005JC002939

Torrence C, Compo GP (1998) A practical guide to wavelet analysis. Bull Am Meteorol Soc 79:61–78. doi:10.1175/1520-0477(1998)079<0061:APGTWA>2.0.CO;2

Xie SP (1999) A dynamic ocean-atmosphere model of the tropical Atlantic decadal variability. J Clim 12:64–70

Xie SP, Carton JA (2004) Tropical Atlantic variability: patterns, mechanisms, and impacts. In Earth's climate: the ocean-atmosphere interaction. Geophys Monogr Ser 147:121–142

Yamagata T, Iizuka S (1995) Simulation of the tropical thermal domes in the Atlantic: a seasonal cycle. J Phys Oceanogr 25:2129–2140. doi:10.1175/1520-0485(1995)025<2129:SOTTTD>2.0.CO;2

Yu L, Jin X, Weller RA (2006) Role of net surface heat flux in seasonal variations of sea surface temperature in the tropical Atlantic Ocean. J Clim 19:6153–6169. doi:10.1175/JCLI3970.1

Zebiak SE (1993) Air-sea interaction in the equatorial Atlantic region. J Clim 6:1567–1586. doi:10.1175/1520-0442(1993)006<1567:AIITEA>2.0.CO;2